# Integrin β1 activation by micro-scale curvature promotes pro-angiogenic secretion of human mesenchymal stem cells

Zhengdong Li, [‡ab] Weiwei Wang,[‡a] Xun Xu,[‡ab] Karl Kratz,[ac] Jie Zou,[ab] Liudmila Lysyakova,[ac] Matthias Heuchel,[a] Andreas Kurtz,[d] Manfred Gossen,[a] Nan Ma*[abc] and Andreas Lendlein*[abc]

[a] Institute of Biomaterial Science and Berlin-Brandenburg Center for Regenerative Therapies, Helmholtz-Zentrum Geesthacht, Kantstraße 55, 14513 Teltow, Germany; E-mail: nan.ma@hzg.de, andreas.lendlein@hzg.de

[b] Institute of Chemistry and Biochemistry, Freie Universität Berlin, Takustraße 3, 14195 Berlin, Germany

[c] Helmholtz Virtual Institute „Multifunctional Biomaterials for Medicine“, Kantstraße 55, 14513 Teltow, Germany

[d] Charité – University Medicine Berlin, Augustenburger Platz 1, 13353 Berlin, Germany

[‡] These authors contributed equally to this work.

## Abstract

Fine tuning of the substrate properties to modulate mesenchymal stem cell (MSC) function has emerged as an attractive strategy to optimize their therapeutic potential. In the context of mechanotransduction process, the conformational change of integrin (integrin activation) plays a critical role to perceive and transmit various signals. In this study, polymeric cell culture inserts with defined bottom roughness were fabricated as a model system for cell cultivation. We showed the conformational change of integrin and its downstream signaling cascade of human adipose-

derived mesenchymal stem cells (hADSCs) could be modulated by the curvature of the cell-material interface. The curvature of substrate surface with a roughness in the size range of a single cell could strongly increase high-affinity β1 integrin level of hADSCs without alteration of total β1 integrin level. Further, the integrin downstream FAK/ERK and Rho/ROCK pathways were activated and resulted in upregulated VEGF secretion of hADSCs. Conditioned medium on such a surface exhibited a strong pro-angiogenic effect, with an increased formation of tubular structure, a higher migration velocity of endothelial cells and an enhanced blood vessel density in e*x vivo* hen's egg test-chorioallantoic membrane (HET-CAM). These results highlighted the clinical potential to manipulate topographic features of cell culture substrate, whereby to regulate integrin affinity states and further control MSC functions.

**Key words:** micro-scale curvature, mesenchymal stem cells, integrin activation, FAK, angiogenesis

## 1 Introduction

Mesenchymal stem cells (MSCs) have demonstrated major advantages to meet the clinical requirements including abundance, homing ability, functional plasticity and immunoregulatory properties.[1] Accumulated evidences have proved that MSCs can transmit the cues from their micro-environment such as stiffness,[2, 3] surface topography,[4-8] and external force [9] into biochemical activity, which is referred to mechanotransduction.[10, 11] This opens a promising field of modulating and controlling MSC function simply through mechanical stimuli for improved therapeutic efficacy. Among these stimuli, surface topography/roughness is an effective approach to modulate MSCs. It has been demonstrated that bioceramic scaffolds with micro-nano-hybrid surface topographies could significantly enhance cell attachment and viability, osteogenic differentiation and pro-angiogenic effects of MSCs;[7] and poly(*ε*-caprolactone) surface with a roughness level similar to native bone induced the preferential osteogenic commitment of MSCs.[12] Hence, understanding the molecular mechanisms to further utilize these beneficial effects is of major clinical relevance.

Integrin, as a transmembrane receptor and primary mechanosensor of cells, plays a critical role to perceive various signals during the mechanotransduction process.[13] Integrin is a heterodimer of the non-covalently linked type I transmembrane α and β subunits. A substantial proportion of integrins on cell surface is inactive. Upon extracellular stimulation, integrins undergo a change in conformation and affinity (integrin activation), which allows the recruitment of several cytoplasmic proteins. [14] High-affinity integrins are highly concentrated in the cell's contact points to ECM including focal adhesions and their variants (focal complexes, fibrillar adhesions and podosomes), mediating cell-ECM interactions. As integrins bind both extracellular and intracellular ligands, they regulate the bidirectional transmission of the mechanical and biochemical signals across the cell membrane.[15] On one hand, the 'inside-out' signaling leads to conformational changes in the extracellular domain of integrin, resulting in an increased affinity of integrin to extracellular ligands. This process is termed integrin activation and is regulated by different intracellular activators, such as talin or kindlin, which bind to the cytoplasmic tail of integrin.[16] Once activated, integrin mediates extracellularly the mechanical interaction of cells with ECM, connects to cytoskeletal actin intracellularly via a series of linker proteins, and regulates several important signaling cascades by activating protein tyrosine kinases such as focal adhesion kinase (FAK) and Src-family kinases.[17] On the other hand, integrin can transmit the signals into the cells through 'outside-in' signaling, providing extracellular information including its adhesive state and the surrounding environment. Both, the conformational change and the clustering of integrin contribute to the 'outside-in' signaling and can lead to a series of cellular response to extracellular matrix such as cell adhesion, cytoskeletal structure, migration, gene expression, cell survival, proliferation, and differentiation.[15] Therefore, understanding the integrin conformation/affinity change and its downstream pathways would be of great importance to clarify the mechanotransduction mechanism, providing valuable information for design and development of novel substrates potentially used as cell culture device or implants.

In this study, we hypothesized that tuning the curvature of cell-material interface might be an effective approach to regulate β1 integrin affinity and its downstream signaling pathways, and further modulate MSC behavior and function. As a cell culture device, polystyrene (PS)-based inserts with three roughness levels on the bottom were fabricated for culturing hADSCs (Fig. 1A-D). As the PS used here is an amorphous polymer, it can provide a homogeneous surface. A smooth surface (PS-000) was used here as a control. A surface (PS-160) with a roughness level comparable

to hADSC dimension (~ 100 μm in adhesion) was expected to regulate the MSCs at the single cell level via its local curvature, while a surface (PS-320) with a roughness surpassing hADSC size might be capable of modulating cell clusters. The cellular responses of hADSCs to the roughness including their morphology, surface markers and proliferation were evaluated. The VEGF secretion was quantified, and the effect of the conditioned media from the cell cultures on angiogenesis was examined both *in vitro* using human umbilical vein endothelial cells (HUVECs) and *ex vivo* via the hen's egg test - chorioallantoic membrane (HET-CAM) assay. In particular, we studied the underlying mechanism, through which the VEGF secretion of hADSCs was regulated by the micro-scale roughness. Our results demonstrated that the PS-160 surface with a roughness in the range of cell size could elevate high-affinity β1integrin level without an alteration of total β1 integrin level, resulting in significantly promoted VEGF secretion of hADSCs (as illustrated in Fig. 1E).

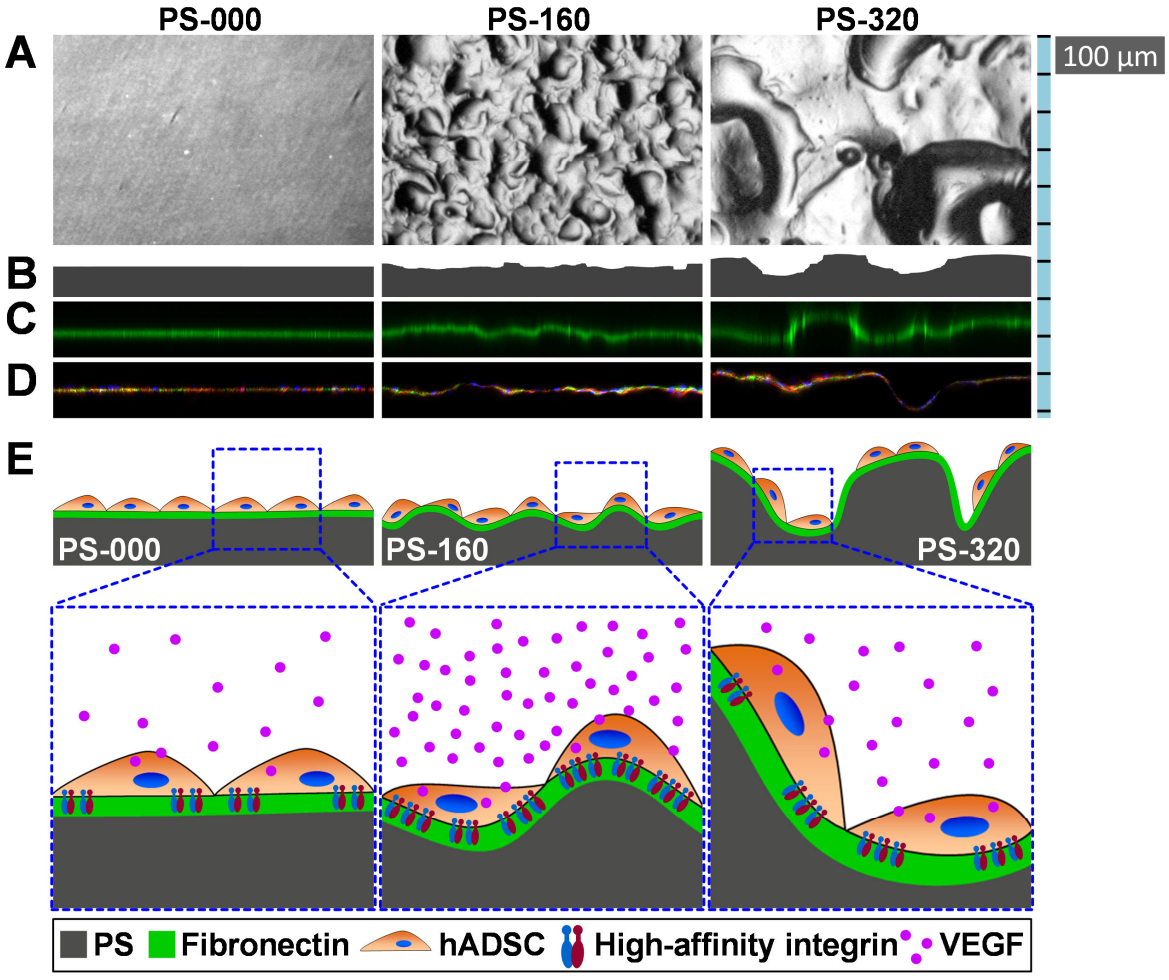

Fig. 1. Modulating VEGF secretion of hADSCs via micro-scale surface curvature. (A) Phase contrast microscope images showing the top-view of the insert bottoms with different roughness. (B) Side-view surface profiles of the insert bottoms determined by optical profilometry. (C) The inserts were coated with fibronectin to facilitate cell adhesion and the immunofluorescent staining images demonstrated the distribution of pre-coated fibronectin. The absorbed fibronectin formed the homogeneous layers (green) on all surfaces according to the cross-sectional view of the orthoimages. (D) The hADSCs were cultured on fibronectin-coated surfaces for 14 days followed by fluorescence staining to detect the actin cytoskeleton (red), nuclei (blue), and fibronectin (green) using a confocal laser scanning microscope. (E) Schematic diagram illustrating that the micro-scale curvature of the substrate surface could influence hADSC shape and morphology, and modulate VEGF secretion via integrin mediated mechanotransduction.

## 2 Experimental Section

### 2.1 Cell culture inserts

PS (Type 158K, BASF, Germany) with a number average molecular weight of $M_n$ = 109.000 g·mol$^{-1}$ was used without any further purification to prepare the inserts fitting standard 24-well tissue culture plates via injection molding as described before.[18, 19] The (micro)curvature of the injection molded polystyrene cell culture inserts was controlled by the utilization of metal cylinders having different micro surface roughness in a custom made mold. Three differently structured cylinders were utilized to manufacture the inserts with different types of bottom roughness: a cylinder with a polished contact surface (PS-000), and two cylinders with micro-structured surfaces according to the standard of German Institute for Standardization (DIN 16747: 1981-05), M30 (PS-160) and M45 (PS-320). The prepared inserts were sterilized by gas sterilization (gas phase: 10% ethylene oxide, 54 ºC, 65% relative humidity, 1.7 bar, 3 h of gas exposure time and 21 h of aeration phase). Before using the prepared inserts for hADSC cultivation, the inserts were coated with human fibronectin (Sigma-Aldrich, St. Louis, MO, USA) to enhance the cell attachment. For each insert, 300 µl of fibronectin solution (10 µg/ml in PBS) was added and incubated at 37 ºC for 1 h, followed by washing three times with PBS.

Optical profilometry and atomic force microscopy was employed for characterization of the PS surface structures. An optical profilometer type MicoProf 200 (FRT - Fries Research & Technologie GmbH, Bergisch Gladbach, Germany) equipped with a CWL 300 μm chromatic white-light sensor was utilized for determination of the arithmetic average roughness ($R_a$) at micro scale and the mean spacing between the peaks ($S_m$) of sterile PS substrates (details are given in Supporting method S1). Surface topography investigations and nanoindentation experiments were conducted with an atomic force microscope MFP-3D Bio-AFM (Asylum Research, Santa Barbara, CA, U S A) with PS substrates in the dry state at ambient conditions (for details see Supporting method S2).

### 2.2 Cell culture and conditioned medium collection

hADSCs were isolated from human adipose tissue as described previously.[4] The adipose tissue was obtained by abdominal liposuction from a female donor after informed consent (No.: EA2/127/07; Ethics Committee of the Charité - Universitätsmedizin Berlin, approval from 17.10.2008). The hADSCs were expanded in human adipose-derived stem cell medium (ADSC$^{TM}$ growth medium, Lonza, Walkersville, MD, USA) and then stored in liquid nitrogen. The cells were recovered and maintained in a cell culture incubator (37 °C, 5% $CO_2$), and were used from passage three for all experiments. The HUVECs (Lonza, Walkersville, MD, USA) were cultured in endothelial cell growth medium (EGM$^{TM}$, Lonza, Walkersville, MD, USA) in a cell culture incubator.

The conditioned media of hADSC cultures derived from different surfaces were collected at the indicated time points. $1.0 \times 10^4$ cells were seeded per insert. 24 h before medium collection, the growth medium was replaced with 500 μl of fresh ADSC$^{TM}$ medium. Collected conditioned media were stored at -20 ºC for further experiments.

### 2.3 Cell size and contact area to the substrate

To study the cell size and contact area to the material surface, hADSCs were seeded ($1.0 \times 10^4$ cells for each insert) and fixed after 3 days of culture to perform the fluorescence staining. Four fluorescent images in each group were then analyzed using ImageJ software (National Institutes of Health, USA) to calculate the cell size (2D spreading area). First, the total cell covered area was

calculated, and the cell number was determined by counting the nuclei. Then the 2D spreading area of single cells was calculated by dividing the total cell covered area with the cell number. However, it should be noted that such an analysis becomes difficult at a higher cell density, due to the proximity of the cells.

The true cell size or contact area to the rough surfaces (3D spreading area) was further calculated based on the result of 2D spreading area. The ratio of surface area ($S_{AR}$) between the rough surfaces and smooth surface was calculated via model-based analysis ($S_{AR}$, PS-160/PS-000 = 1.18; $S_{AR}$, PS-320/PS-000 = 3.24; see supporting method S4 and Fig. S6). Assuming that the cells were distributed randomly on the rough surfaces, the following equation was applied: 3D spreading area = 2D spreading area × $S_{AR}$. However, randomly distributed hADSCs were only observed on PS-160, but not on PS-320.

### 2.4 Fluorescence staining and laser scanning microscopy

$1.0 \times 10^4$ hADSCs were seeded into each insert. At the indicated time points for staining, the cells were fixed with 4% paraformaldehyde for 20 minutes, permeabilized with 0.1% Triton X-100 for 10 minutes and blocked with 1% BSA for 30 minutes. Vinculin was stained with mouse anti-human vinculin monoclonal antibody (Merck Millipore, Darmstadt, Germany) and Alexa Fluor® 488 labeled IgG antibody (Life Technologies, Darmstadt, Germany). F-actin was stained with Alexa Fluor® 555 Phalloidin (Life Technologies, Darmstadt, Germany). The cell nuclei were stained with Hoechst 33342 (NucBlue® Live Reagent, Life Technologies, Darmstadt, Germany). To detect the pre-coated fibronectin on different surfaces and study its organization during cell culture, fibronectin was stained with Anti-Fibronectin antibody-Alexa Fluor® 488 (Abcam, Cambridge, United Kingdom). After staining, the samples were scanned using a confocal laser scanning microscope (LSM 780, Carl Zeiss, Jena, Germany) using the mode of z-stack multilayer scanning, and the images were processed using ZEN 2012 software (Carl Zeiss, Jena, Germany). The cross-sectional view of the orthographic images was used to study the distribution of the pre-coated fibronectin, and the fluorescence intensity was analyzed using ImageJ software (National Institutes of Health, USA) to compare the adsorption density of fibronectin on different surfaces and in different areas. The top-view images of the samples were processed by Maximum Intensity

Projection to study the cell morphology, fibronectin organization and focal adhesions, and further analyzed to study the cell size and contact area to the material surfaces.

In addition, to observe the cell-material interface, the tilted-view images were taken by tilting the samples to make a 25° angle between the objective and the material surface (Fig. S3A). A confocal laser scanning microscope (LSM 780, Carl Zeiss, Jena, Germany) was applied to scan the samples using the mode of z-stack multilayer scanning. The 3D images were then reconstructed based on the single layer scanning images using the ZEN 2012 software (Carl Zeiss, Jena, Germany).

### 2.5 Flow cytometry

$1.0 \times 10^4$ hADSCs were seeded into each insert. After 14 days of culture, the cells were harvested and stained with a Human MSC Analysis Kit (Stemflow$^{TM}$, BD Biosciences, Heidelberg, Germany) according to the manufacturer's instruction to examine the cell surface markers. To quantify the β1 integrin, hADSCs were cultured in the inserts. After four days, the cells were harvested using StemPro Accutase® (Thermo Fisher Scientific, Bonn, Germany) for 2 minutes at 37 °C, fixed with 4% (w/v) paraformaldehyde for 15 minutes. To detect β1 integrin in the whole cells (surface and cytoplasm), the cells were permeabilized with 0.1 % (w/v) Triton X-100 in PBS for 10 minutes. To detect β1 integrin on the cell surface, no permeabilization step was applied. After blocking with 1% (w/v) BSA for 30 minutes, the activated or total β1 integrin was stained using monoclonal mouse anti-human integrin beta-1 antibody (HUTS-4, Millipore, Darmstadt, Germany) or total integrin beta-1 antibody (Abcam, Cambridge, UK), and Alexa Fluor® 488 labeled IgG antibody (Life Technologies, Darmstadt, Germany). A flow cytometer (MACSQuant®, Miltenyi Biotec, Bergisch Gladbach, Germany) was used to analyze the cells, and the data were processed using Flowjo software (Tree Star Inc., Ashland OR, USA).

### 2.6 Enzyme-linked immunosorbent assay (ELISA)

The expression levels of VEGF, phosphorylated FAK (pFAK), total FAK (tFAK) and phosphorylated extracellular signal-regulated kinase (pERK) of hADSCs growing on different surfaces were quantified by ELISA. The VEGF concentration in the conditioned medium was determined using a human VEGF-A ELISA kit (Thermo Fisher Scientific, Bonn, Germany). The concentration of pFAK, tFAK and pERK in the cell extract were measured using the pFAK

(pY397), tFAK and pERK (ERK1[pTpY202/204] and ERK2[pTpY185/187]) ELISA kits (Life Technologies, Darmstadt, Germany). The amount of total protein in the cell extract was determined using a BCA protein assay kit (Thermo Fisher Scientific, Bonn, Germany) to normalize the expression levels of the proteins of interest.

### 2.7 Tube formation and migration of HUVECs

The tube formation and migration of HUVECs were tested using the conditioned media collected from the hADSC cultures on different surfaces. To assess the tube formation of HUVECs, a 24-well tissue culture plate was first coated with Geltrex® Matrix solution (Life Technologies, Darmstadt, Germany; 200 µl per well) according to the given protocol. Thereafter $6.0 \times 10^4$ HUVEC cells per well were seeded on the matrix. For each well, 500 µl of conditioned medium collected at day 14 was applied for cell culture. The cells were stained with calcein (Life Technologies, Darmstadt, Germany) after 24 h of incubation, and the formed tubes were visualized using a fluorescence microscope (AxioSkop, Carl Zeiss, Jena, Germany). In each well, the images were taken in randomly selected observation fields and the number of the complete rings was counted.

The migration of HUVECs was tracked using a time-lapse imaging microscope (IX81 motorized inverted microscope, Olympus, Hamburg, Germany) equipped with a bold line cage incubator to maintain cell growth in a humidified atmosphere (37 °C, 5% $CO_2$). HUVECs were seeded in a 24-well tissue culture plate with the number of $2.0 \times 10^4$ cells per well. After 24 h of culture, the medium was replaced with the conditioned medium collected at day 14 (500 µl per well), and the cell migration was recorded up to 24 h. The migration trajectories and velocity were analyzed using ImageJ software (National Institutes of Health, USA) combined with the software plug-ins “manual tracking” and “chemotaxis and migration tool” (ibidi GmbH, Martinsried, Germany).

### 2.8 HET-CAM assay

HET-CAM assay was performed to assess the effect of the conditioned medium on angiogenesis. The fertile VALO SPF eggs of white Leghorn species (Lohmann Tierzucht GmbH, Cuxhaven, Germany) were bred at 37°C and 65% humidity for 8 days in the breeding incubator (BSS 300 MP GTFS, Grumbach GmbH, Asslar, Germany). Before the test, the position of the air bubbles was

marked under a shell lamp, and the marked upper part of the egg shell was removed. Then the exposed inner membrane was moistened with 0.9% NaCl and carefully removed. After that, 500 µl of conditioned medium collected at day 14 was dropped on the chorioallantoic membrane. Images were taken at the starting point, 24 h and 48 h later, respectively, using a stereomicroscope (MZ16A, Leica, Wetzlar, Germany). The vessels crossing the middle line of the image were counted, and the fold increase of the vessel density was calculated (fold increase = vessel density after 24 or 48 h / vessel density at starting point).

### 2.9 Inhibition experiment

FAK inhibitor PF-573228 and rho-associated coiled-coil-containing protein kinase (ROCK) inhibitor Y-27632 (both from Sigma-Aldrich, St. Louis, MO, USA) were used in the inhibition experiment. $1.0 \times 10^4$ hADSCs were seeded per insert. After 10 days of culture PF-573228, Y-27632 or both were added at a final concentration of 10 µM each. The inhibitor-containing medium was changed once at day 12. The conditioned medium was collected at day 14 and the cells were lysed to extract the proteins.

### 2.10 Statistics

The number of replication for experiments was larger than three as indicated respectively in the figure legends for each assay, and data are expressed as mean ± standard deviation. Statistical analysis was performed using two-tailed independent samples t-test, and a significance level (Sig.) $< 0.05$ was considered to be statistically significant.

## 3 Results and discussion

### 3.1 Surface characterization

Three substrates were designed and prepared: PS-000 smooth surface, PS-160 with a surface roughness in the range of cell size, PS-320 with a roughness surpassing hADSC size. The insert bottom was analyzed by optical profilometry measurements and the obtained results are listed in Table S1. PS-000 exhibited a $R_a$ value of 0.13 ± 0.07 µm, while higher $R_a$ values of 4.17 ± 0.17 µm and 25.4 ± 3.8 µm were obtained for the micro-rough surfaces PS-160 and PS-320. The $S_m$

value of PS-160 was 164 ± 16 μm, comparable to the dimension of single hADSC, while for PS-320 a higher $S_m$ of 316 ± 36 μm was found. The nanoscale roughness obtained by atomic force microscopy exploring a scan size of 2 × 2 $\mu m^2$ revealed average $R_a$ values less than 15 nm for the different surfaces. As the surfaces were coated with human fibronectin prior to cell seeding, the fibronectin adsorption and distribution were evaluated. The coated fibronectin formed a homogenous layer on the insert bottom (Fig. 1C). The fibronectin density was at a similar level on different surfaces and in different areas according to the fluorescence intensity analysis. AFM investigations utilizing nanoindentation technique showed almost similar local mechanical properties of the different substrates. Here, a Young's modulus of 31 ± 2 GPa was found for PS-000, while values of 30 ± 5 and 29 ± 2 GPa were obtained from nano-indenting the top of the hills of the rough samples PS-160 and PS-320 (Table S1).

### 3.2 hADSC proliferation, surface markers and morphology

We found the initial cell attachment after 24 h was similar on all surfaces (Fig. S1A), which was different to the result reported by Bigerelle *et al.* In their study, the bone marrow MSCs showed a lower attachment on the surface with the roughness relevant to the cell size.[20] The possible reasons for this discrepancy might be the surface chemistry of the cell culture materials employed, as we used fibronectin-coated PS compared to the titanium surfaces used in their study. Similarly, no effect of surface roughness on the proliferation rate of hADSCs was observed. The proliferation activity of the cells on different surfaces was similar during 2 weeks of cultivation (Fig. S1A). After 14 days of culture, no change of surface marker expression was observed, independent of the roughness of the culture surface. MSC markers were well preserved and non-MSC markers were not detected, demonstrating that the surface curvature has no influence on hADSC surface markers (Fig. S1B).

Immunofluorescent staining was performed to investigate the cell morphology. After 3 days of cell culture, the analysis based on fluorescent images showed that hADSCs presented a smaller 2D projection size but a similar effective spreading area in 3D on PS-160, as compared to the cells on smooth surface (Fig. 2), suggesting PS-160 surface could effectively modulate hADSC size and shape. In addition, distinct difference was observed in cells on different surfaces with respect to their orientation, distribution, F-actin arrangement, and fibronectin organization (Fig. S2). The

cells on PS-000 surface showed a highly aligned cell orientation and actin cytoskeleton. In contrast, cells and their stress fibers on PS-160 and PS-320 were less orientated. The fibronectin organization by the cells was affected by the surface curvature. Most fibronectin localized beneath the cells, and an increase in fibronectin fibrils around the cell periphery was observed. Notably, the cells on PS-320 were less homogeneously distributed, as compared to those on PS-000 and PS-160.

To further study the interaction of cells and materials, the stained samples were observed from a tilt angle (Fig. S3A). This approach could overcome the limitations of normal top-view method, as the images of cell-material interface could be generated with high resolution. The single layer scanning images indicated that the cells formed a monolayer on all surfaces (Fig. 1D). Accordingly, a smooth cell layer was observed on PS-000, whereas the rougher cell layers were found on PS-160 and PS-320 (Fig. S3B).

Moreover, our model-based analysis indicated that the cells on PS-160 and PS-320 surfaces might perceive the different cues of local curvature (Fig. S6 and Supporting method S4). Compared to PS-320, the PS-160 surface with a roughness in the range of cell size has apparently a larger portion of surface with optimal curvature properties for *in situ* regulation of hADSC properties. Accordingly, when hADSCs attached on PS-160 a large fraction of cells could be affected by the local curvature. In contrast, the larger portion of relatively smoother surface in the range of cell size on PS-320, for example the broad valleys, flat peaks or gentle slopes, may in average reduce the effect of local curvature experienced by the given hADSCs.

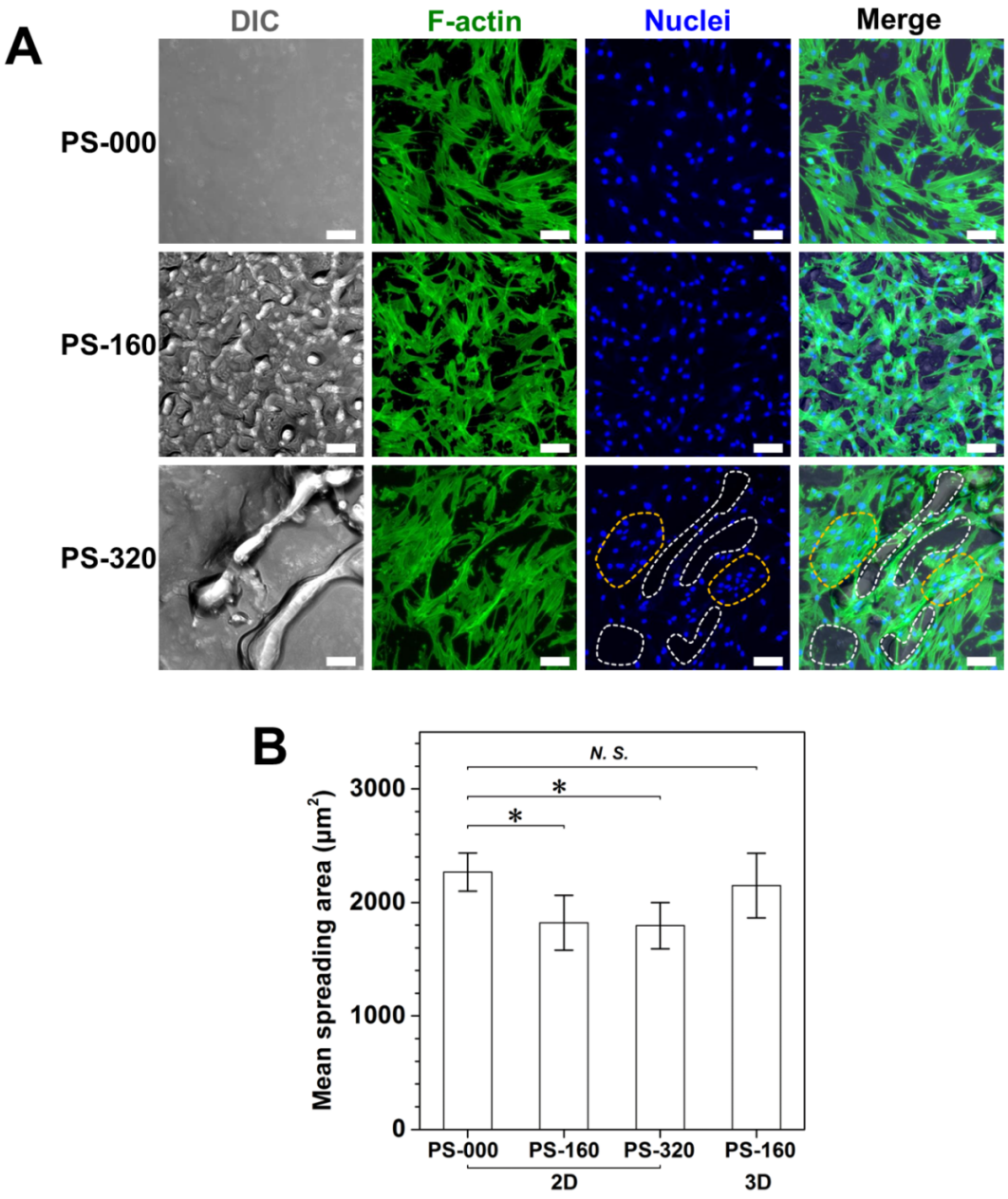


Fig. 2. hADSC size and contact area to the material surfaces. (A) Representative images of fluorescently stained hADSCs on different substrates (bar = 100 μm). Inhomogeneous cell distribution was observed on PS-320 surface, as indicated by the areas enclosed by the dash-lines (white: low cell density; yellow: high cell density). (B) 2D and 3D spreading area of single hADSCs on different surfaces. The quantification was based on 4 randomly selected images (*Sig < 0.05).

### 3.3 Enhancement of integrin mediated FAK signaling by micro-scale curvature

Cells receive various mechanical signals via their transmembrane receptors (such as integrin) from their micro-environment, assemble focal adhesions accordingly, and launch a series of intracellular biochemical signaling events.[21] To study the cell-material interaction and to determine the potential mechanism, the focal adhesion-related protein components were investigated. Flow cytometry analysis was performed to quantify activated and total β1 integrin in hADSCs cultured on different substrates. Significantly higher levels of activated β1 integrin on cell surface and in the whole cells were observed in PS-160 group at day 4, as compared to the cells on PS-000 and PS-320. The total β1 integrin was at a similar level for these three groups (Fig. 3A). These results were further confirmed by immunofluorescence staining and western blot analysis (Fig. S4). The focal adhesion complex formation was examined by immunofluorescent staining of vinculin. After 4 days of culture, hADSCs on PS-160 surface formed more focal adhesions than on PS-000 and PS-320 (Fig. 3B). These results suggested that PS-160 substrate could enhance the β1 integrin activation of hADSCs without alteration of the total β1 integrin level. Given that the surface chemistry of these substrates was identical, the enhanced β1 integrin activation might be predominantly due to the physical features of PS-160 surface. We speculated that the PS-160 roughness with a comparable scale to cell size might provide appropriate topographic cues such as the local curvature, which could be perceived by cells to modulate the integrin mediated adhesion. This observation is consistent with the previous findings that the focal adhesion complexes of MSCs were primarily formed at the regions of local curvature when they grew on 2D micro-patterns or in 3D micro-wells.[4, 22] Notably, the difference in fibronectin remodeling by hADSCs on different surfaces was observed here (Fig. S2). Fibronectin remodeling is dynamically related with integrin activation. On the one hand, extracellular fibronectin assembly requires the participation of integrin that recognizes the RGD and synergy sequences in fibronectin.[23] On the other hand, the fibronectin density can affect the activation of cell surface integrin.[24]

The engagement of integrin with its extracellular ligand can activate various intracellular signaling components. Multiple structural and signaling proteins are recruited to focal adhesions upon cell adhesion to ECM. Among these proteins, FAK is one of the most prominent signaling molecules, which is composed of a central kinase domain flanked by an N-terminal FERM domain and a C-terminal FAT domain.[25, 26] Intracellularly, the autophosphorylation of FAK at Y397 can be

initiated by the binding of integrins to ECM and their clustering. Y397 is the most important phosphorylation site since the kinase activity of FAK can be fully activated via its phosphorylation. Phosphorylation at Y397 creates a high-affinity binding site for the Src-homology 2 (SH2) domain of Src family kinases. The recruitment of Src by FAK leads to a conformational activation of Src, which consequently promotes the Src-dependent phosphorylation of FAK at other tyrosines.[27] In this study, at day 4 the ratio of phosphorylated to total FAK (pY397FAK/tFAK) was significantly higher in the PS-160 group as demonstrated by ELISA result, and this elevated FAK phosphorylation was maintained at least 14 days (Fig. 3C). Further, a higher FAK phosphorylation level in cells on PS-160 than on PS-000 and PS-320 was evidenced by the immunostaining and western blot results (Fig. S5).

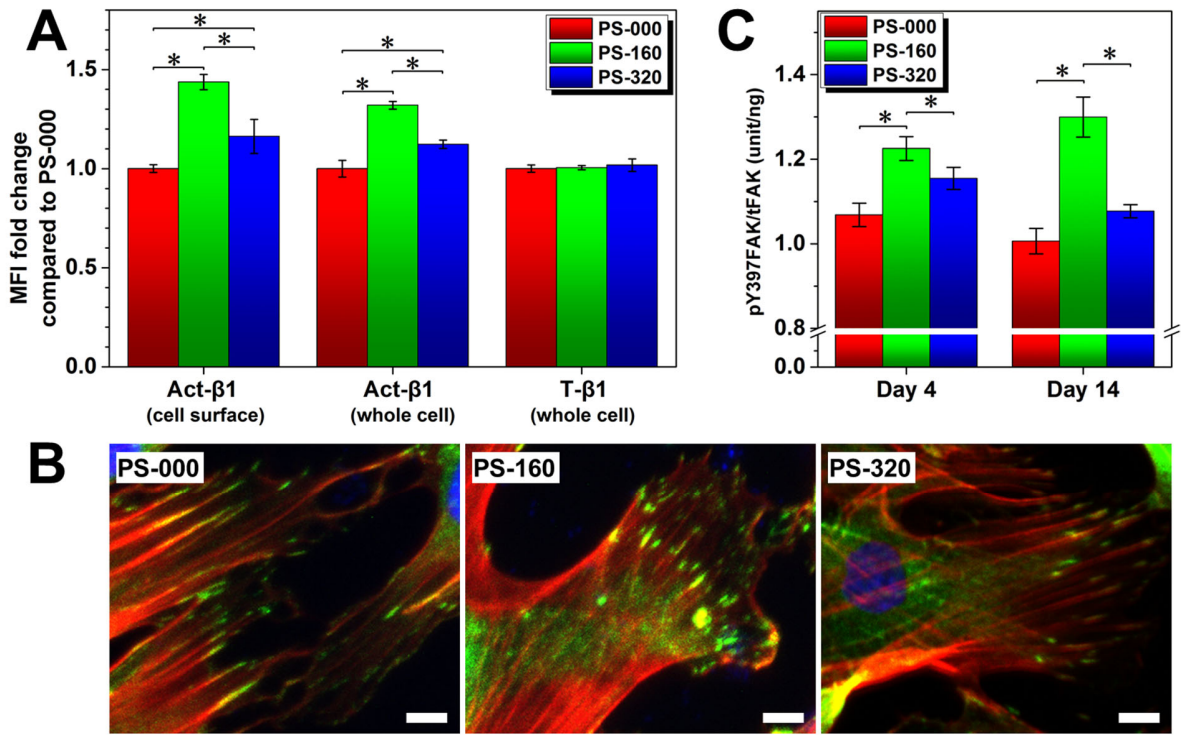


Fig. 3. PS-160 substrate enhanced β1 integrin activation, focal adhesion formation and FAK phosphorylation. (A) Activated β1 integrin (Act-β1) and total β1 integrin (T-β1) were quantified using flow cytometry, and the result was expressed as the fold change of mean fluorescence intensity (MFI) compared to PS-000 group. hADSCs on PS-160 showed the higher levels of activated β1 integrin on cell surface and in the whole cells compared to cells on PS-000 and PS-320. (B) Representative laser scanning microscopic images showed the formation of a higher

number of focal adhesions on PS-160 than on PS-000 and PS-320 (red: F-actin; green: vinculin; blue: nuclei; bar = 10 μm). (C) FAK phosphorylation was induced by PS-160 surface to a significantly higher level than by PS-000 and PS-320. Cells cultured in 3 independent inserts of each group were analyzed (*Sig < 0.05).

### 3.4 Promotion of VEGF secretion by micro-scale curvature

Upon integrin engagement, the activation of FAK and Src can subsequently activate the downstream mitogen-activated protein kinase (MAPK)/ERK pathway. The phosphorylation of FAK at Y925 facilitates the SH2-mediated binding of Grb2 adaptor protein, which can activate the Ras-Raf-MEK-ERK signaling and promote VEGF expression in tumor cells.[28] Here, the VEGF secretion of hADSCs on different surfaces was quantified and the pro-angiogenic effect of cell secretome was assessed.

First, the VEGF concentration in the conditioned media of hADSCs cultured on different surfaces was quantified at day 4, 7 and 14. Markedly, hADSCs cultured on PS-160 surface secreted more VEGF than those on PS-000 and PS-320 at all analyzed time points. At day 4, the VEGF concentration in the medium of PS-160 culture was around 40% and 50% higher than that in PS-000 and PS-320 cultures, respectively. After 2 weeks, the VEGF concentration in the medium of PS-160 culture still remained highest, around 80% and 20% increase over that in PS-000 and PS-320 groups, respectively (Fig. 4A). Further, to challenge the possible biological relevance of elevated VEGF in the hADSC secretome as a result of culturing cells on surfaces with micro-scale curvature, the pro-angiogenic effect of the conditioned media was assessed by an *in vitro* assay. The conditioned medium derived from hADSCs cultured on PS-160 surface could significantly enhance the tube formation of HUVECs compared to accordingly conditioned media from PS-000 and PS-320 surfaces (Fig. 4B). To evaluate the HUVEC migration driven by the conditioned media, the cells were cultured in the conditioned media and their migration track was recorded using a time-lapse microscope. The HUVEC migration velocity was significantly elevated when grown in conditioned medium derived from PS-160 surface. The cells in PS-160 medium moved around 1.4 and 1.3 times as fast as the cells in PS-000 and PS-320 media, respectively (Fig. 4C). A HET-CAM assay was performed to further evaluate the pro-angiogenic capacity of conditioned media under *ex vivo* condition. A higher number of newly formed vessels was observed on the

chorioallantoic membrane treated by PS-160 medium than by PS-000 and PS-320 media (Fig. 4D). Compared to the initial state, the PS-160 medium resulted in the highest fold increase of vessel density after 24 h, as compared to the PS-000 and PS-320 media. After 48 h of treatment, there was still a significant higher increase of the vessel density in the PS-160 medium treated group, consistent with the finding in the *in vitro* tubulogenesis assay. Our findings on the modulation of angiogenic capacity of freely migrating MSCs by local curvature are in part supported by the latest report using discrete adhesive micropatterns, with varying aspect ratio and local curvature, to stimulate immobilized MSCs the angiogenic factor secretion.[29] It should be noted that the enhanced pro-angiogenic effect of the conditioned medium from PS-160 might not only be due to the VEGF upregulation but also a synergistic effect with other growth factors. Further studies are necessary to clarify the secretion profile of angiogenic factors at different interface curvatures.

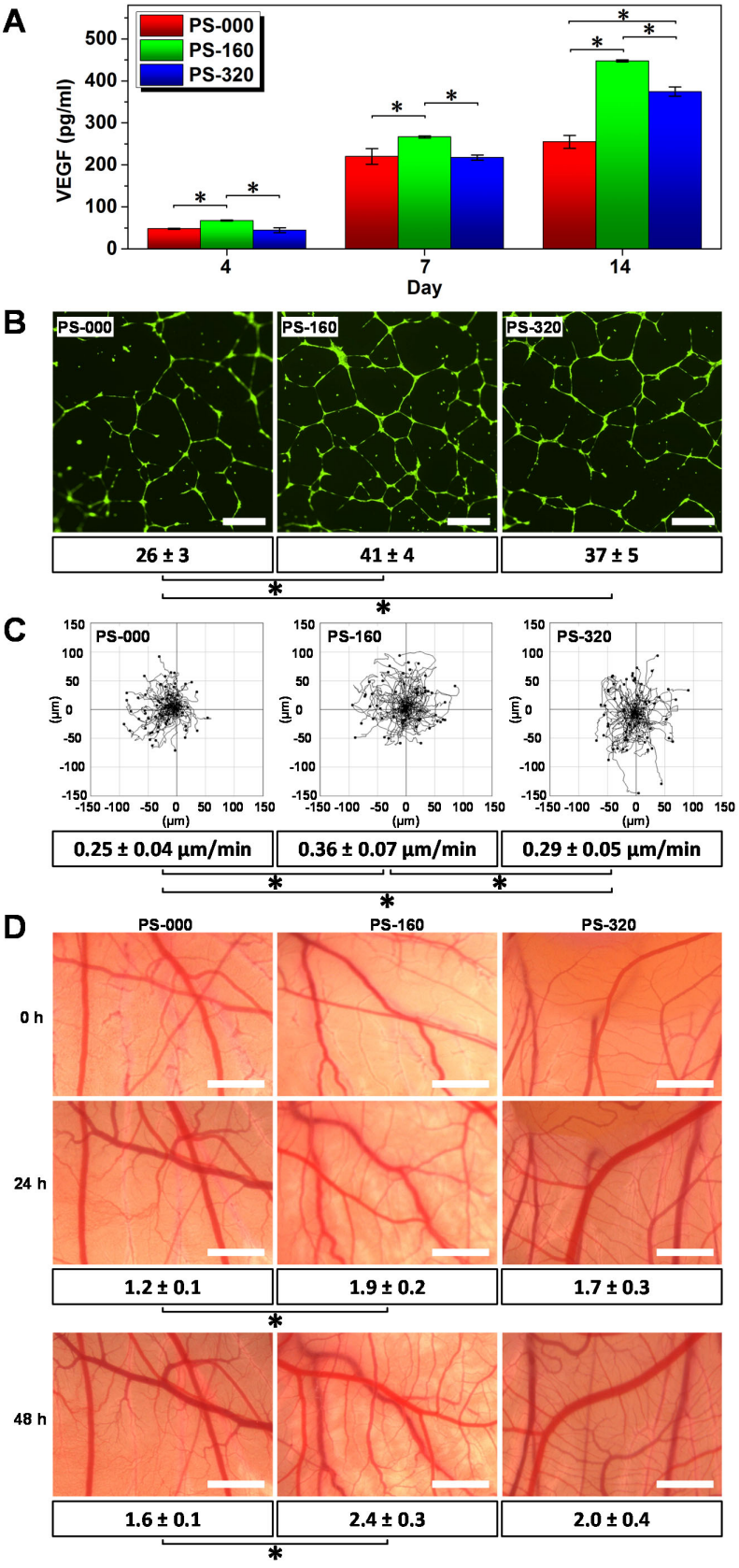
A
PS-000
PS-160
PS-320
VEGF (pg/ml)
0
100
200
300
400
500
4
7
14
Day
*
B
PS-000
PS-160
PS-320
26 ± 3
41 ± 4
37 ± 5
C
PS-000
PS-160
PS-320
(μm)
0.25 ± 0.04 μm/min
0.36 ± 0.07 μm/min
0.29 ± 0.05 μm/min
D
PS-000
PS-160
PS-320
0 h
24 h
48 h
1.2 ± 0.1
1.9 ± 0.2
1.7 ± 0.3
1.6 ± 0.1
2.4 ± 0.3
2.0 ± 0.4

Fig. 4. PS-160 substrate promoted VEGF secretion of hADSCs, and enhanced pro-angiogenic effect of conditioned medium. (A) VEGF secretion of hADSCs on PS-160 surface was induced to a higher degree than on PS-000 and PS-320 surfaces. Cells cultured in 3 independent inserts of each group were analyzed (*Sig < 0.05). (B) Representative images showed the tube formation of HUVECs in conditioned media derived from different surfaces. The HUVECs were stained by calcein. The number of complete rings was counted in 7 randomly selected images to quantify the formed tubes. (C) For cell migration assay, HUVECs cultured in different conditioned media were tracked up to 24 h to generate the migration trajectories and to calculate the migration velocity. For each group, the migration velocity of 60 cells was analyzed. (D) Representative images showed the vessels on the chorioallantoic membrane at the starting point (0 h) and after incubation for 24 and 48 h with the conditioned media. The vessels were accounted based on 5 randomly selected images and the values indicated the fold increase of vessel density as compared to the starting point. (bar = 500 μm; *Sig < 0.05)

### 3.5 VEGF expression regulated by FAK signaling pathway

Small molecule inhibitors related to FAK and ROCK signaling pathways were applied to elucidate the underlying mechanism of micro-scale curvature induced enhancement of VEGF secretion. Without inhibition, the expression levels of both pY397FAK and VEGF were significantly higher in cells growing on PS-160, as compared to cells on PS-000 and PS-320 (Fig. 5A, B). When treated with FAK inhibitor, ROCK inhibitor or both for 4 days, pY397FAK expression was significantly inhibited (Fig. 5A). Accordingly, VEGF levels in the conditioned media were decreased by the inhibitors, as compared to the untreated group (Fig. 5B). In addition, the relative expression levels of related proteins in the untreated hADSCs on PS-160 were determined at different time points. The VEGF expression increased at the earlier stage and reached its peak at day 10. Notably, VEGF amounts determined in the cell culture supernatants largely followed the expression levels of pY397FAK and pERK1/2, and a significant correlation between the expression levels of these three proteins was observed (Fig. 5C). These results indicated the key regulatory function of FAK signaling on VEGF expression of hADSCs in response to surface curvature.

MSCs sense and response to the mechanical environment through the interaction of a signaling network components including FAK, cytoskeletal dynamics and RhoA/ROCK.[9] In the current

study, the participation of RhoA/ROCK pathway in VEGF secretion was observed. The regulation of VEGF secretion by RhoA/ROCK might be through different pathways. First, RhoA/ROCK could stimulate FAK phosphorylation and then activate the ERK signaling. Second, RhoA/ROCK could phosphorylate and activate the downstream target PTEN,[30] which in turn inactivates Akt.[31] This would promote ERK activation as phosphorylation of Raf by Akt can inhibit the activation of the Raf-MEK-ERK cascade.[32] Further studies focusing on the exact function of RhoA/ROCK for mediating VEGF secretion of MSCs will be interesting.

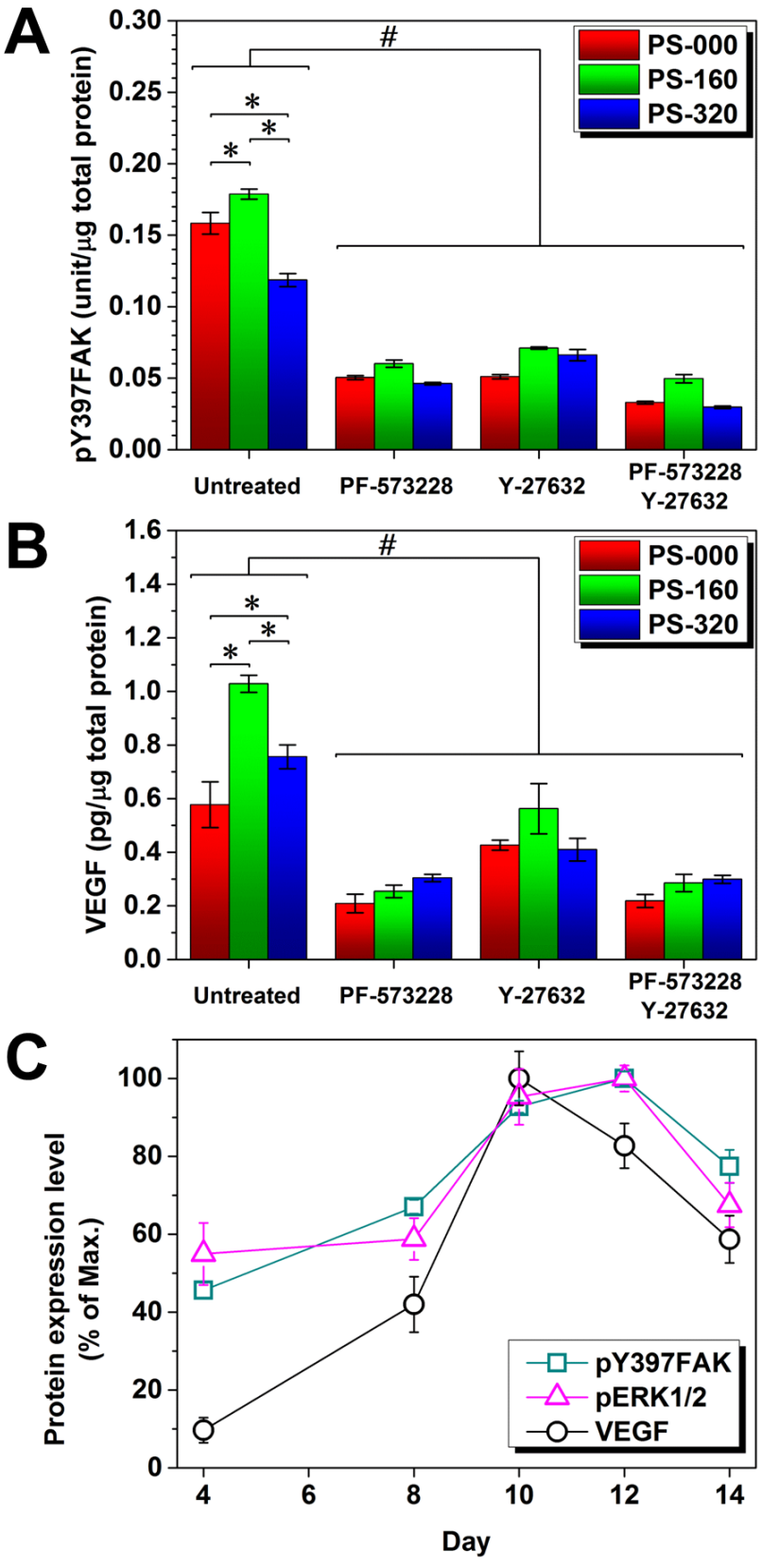
A
pY397FAK (unit/μg total protein)
0.30
0.25
0.20
0.15
0.10
0.05
0.00
#
*
*
*
PS-000
PS-160
PS-320
Untreated
PF-573228
Y-27632
PF-573228
Y-27632
B
VEGF (pg/μg total protein)
1.6
1.4
1.2
1.0
0.8
0.6
0.4
0.2
0.0
#
*
*
*
PS-000
PS-160
PS-320
Untreated
PF-573228
Y-27632
PF-573228
Y-27632
C
Protein expression level
(% of Max.)
100
80
60
40
20
0
4
6
8
10
12
14
Day
pY397FAK
pERK1/2
VEGF

Fig. 5. Modulation of VEGF expression in hADSCs via FAK/ERK signaling. Both pY397FAK (A) and VEGF (B) levels were downregulated when the cells were treated with FAK inhibitor (PF-573228) or/and ROCK inhibitor (Y-27632). Cells cultured in 3 independent inserts of each group were analyzed (*Sig < 0.05 in the untreated group; # Sig < 0.05 for inhibitor treated groups vs untreated group). (C) The expression levels of VEGF, pY397FAK and pERK1/2 exhibited a similar pattern in hADSCs on PS-160 surface and showed a significant correlation according to the analysis of Spearman's rank correlation coefficient (*rs*) and Pearson correlation coefficient (*rp*) (VEGF vs pY397FAK: $rs = 0.9$, $rp = 0.957$; VEGF vs pERK1/2: $rs = 0.9$, $rp = 0.911$; pY397FAK vs pERK1/2: $rs = 1$, $rp = 0.931$). The conditioned media or cell extract samples from 3 independent PS-160 inserts were collected to perform the ELISA analysis. The expression levels of proteins of interest were normalized against the amount of total protein of the cells.

In summary, these results demonstrated that integrin activation and its downstream signaling network were critically involved in hADSC modulation by micro-scale curvature (Fig. 6). When hADSCs attached on the surface with a roughness comparable to the cell dimension, complex changes in the micro-environment will be sensed by the cells. Parameters to consider such as the topography-dependent spectrum of local curvatures, alone or in conjunction with the contacted polymer area, could result in the alteration of cell shape, morphology, cytoskeleton organization and the distribution of adhesion points. Activation of the integrin can be enhanced under these conditions, where their extracellular domains undergo conformation/affinity changes and transmit signals across the cytoplasmic membrane. FAK, as a key component of the integrin triggered signaling pathway, was subsequently activated. The signaling network including FAK and Rho/ROCK may exert the regulatory effect on cell morphology and actin cytoskeleton organization, and activate downstream ERK signaling to enhance VEGF expression. This study pointed at a gateway to control parameters of MSCs critical for their therapeutic potential by specifying cell-material interactions. As a promising cell source in regenerative medicine, MSCs can accelerate tissue regeneration predominantly due to their paracrine activity rather than their direct differentiation,[1, 33-36] due to their low engraftment level and marginal survival rate at the injury site.[37, 38] The regulatory and trophic factors in MSC secretome can exert multiple functions to achieve therapeutic effects in tissue regeneration. Hence, regulating MSC secretion is of great relevance to their clinical applications. Our results suggested that fine-tuning the surface roughness might be an effective and safe approach to improve the therapeutic functions of MSCs. These

results shed light on design and developing biomaterials for both *in vitro* and *in vivo* applications. For instance, *in vitro* preconditioning of MSCs on the surface with such a well-defined topography may improve their therapeutic efficacy after transplantation; or surface topography treatment as a preconditioning approach could be used for producing secretomes. The MSC pre-seeded implant materials with an appropriate surface topography may accelerate tissue regeneration *in vivo*, which might be attributed to elevated level of predominant pro-angiogenic factors in MSC secretome.[39-41]

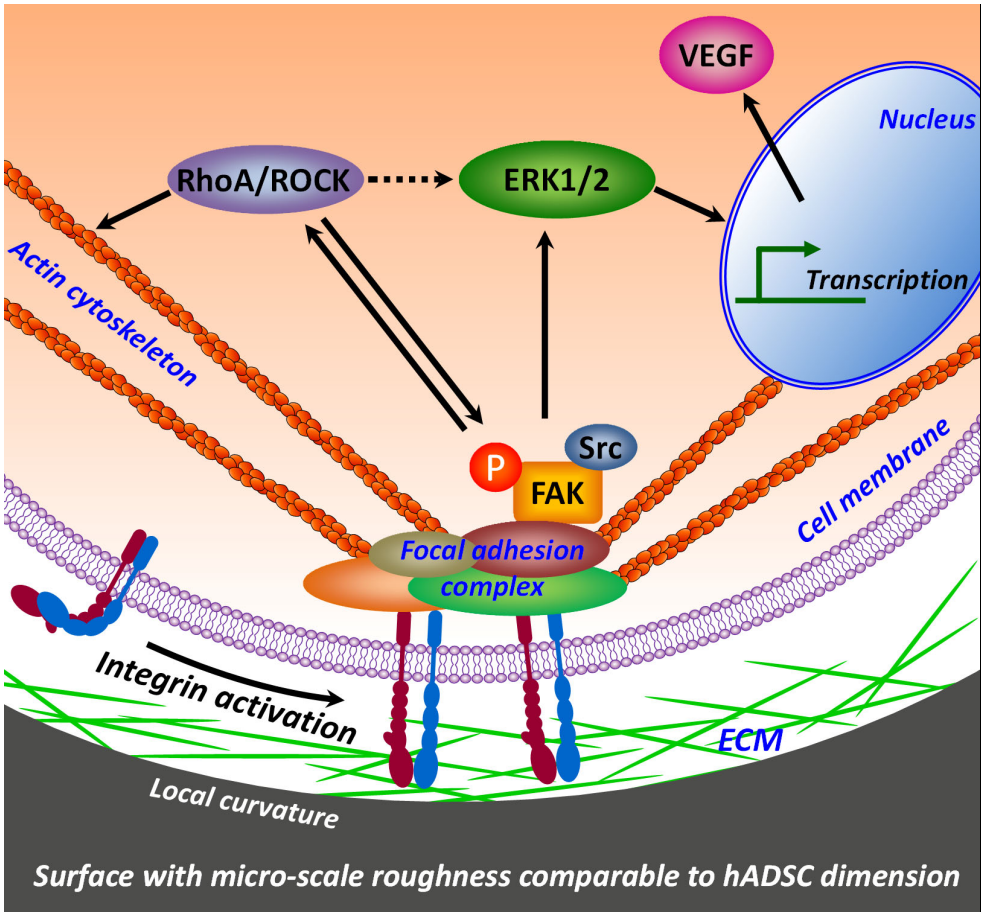


Fig. 6. Proposed model of the regulatory effect of micro-scale curvature on hADSCs. Compared to smooth surface (PS-000) or rougher surface (PS-320), the surface with micro-scale roughness comparable to hADSC dimension (PS-160) could present a larger portion of surface with optimal curvature properties for modulating hADSCs. The cell shape and morphology of hADSCs would

be altered on such a surface. This physical cue of local curvature would induce the enhancement of integrin activation on cell surface, and then activate FAK to form a signaling network. The actin cytoskeleton organization would be modulated accordingly with the involvement of ROCK. And the downstream ERK signaling might be activated, leading to the upregulation of VEGF expression.

## 4 Conclusion

PS inserts with three different types of culture surface roughness (smooth surface: PS-000; with roughness level comparable to hADSC size: PS-160; with roughness level surpassing hADSC size: PS-320) were fabricated to investigate the effect of micro-scale curvature on hADSCs. The cells exhibited different morphology and actin cytoskeleton on different surfaces, but neither their surface markers nor their proliferation were altered by micro-scale curvature. The conditioned medium derived from the substrate with a roughness comparable to hADSC size had a higher pro-angiogenic potential than that from smooth and rougher substrates, which could improve the tube formation and migration of HUVEC cells and enhance the new vessel formation on the chorioallantoic membrane of hen's eggs. Compared to smooth and rougher substrates, the substrate with a roughness comparable to hADSC size could promote VEGF secretion of hADSCs to a significantly higher level, and this effect was regulated through the increased high-affinity β1 integrin level of hADSCs and downstream FAK signaling with participation of RhoA/ROCK. These findings allow a better mechanistic understanding of MSC response to micro-scale curvature. This knowledge might help to design and develop biomaterials with effective and functional surface structures, which can be potentially utilized as implants or *in vitro* cell culture materials, to modulate MSCs and consequently achieve clinical benefits in regenerative medicine.

**Acknowledgements**

The authors acknowledge Robert Jeziorski, Mario Rettschlag for preparation of sterilized PS inserts and Yi Jiang as well as Manuela Keller for technical support. This work was financially supported by the Helmholtz Association of German Research Centers (including Helmholtz Cross Programme Initiative "Technology and Medicine - Adaptive Systems", grant no. VH-VI-423 (Helmholtz Virtual Institute, Multifunctional Biomaterials for Medicine), as well as programme-oriented funding) and the Federal Ministry of Education and Research, Germany, for funding

through the Programme Health Research (grant no. 13GW0098, as well as project number 0315696A "Poly4BioBB").

## Conflict of interest

There are no conflicts of interest to declare.

## References

1. H. O. Kim, S. M. Choi and H. S. Kim, *Tissue Eng Regen Med*, 2013, **10**, 93-101.
2. J. Du, X. F. Chen, X. D. Liang, G. Y. Zhang, J. Xu, L. R. He, Q. Y. Zhan, X. Q. Feng, S. Chien and C. Yang, *P Natl Acad Sci USA*, 2011, **108**, 9466-9471.
3. K. Ye, X. Wang, L. P. Cao, S. Y. Li, Z. H. Li, L. Yu and J. D. Ding, *Nano Lett*, 2015, **15**, 4720-4729.
4. X. Xu, W. W. Wang, K. Kratz, L. Fang, Z. D. Li, A. Kurtz, N. Ma and A. Lendlein, *Adv Healthc Mater*, 2014, **3**, 1991-2003.
5. K. Kulangara, Y. Yang, J. Yang and K. W. Leong, *Biomaterials*, 2012, **33**, 4998-5003.
6. G. Abagnale, M. Steger, V. H. Nguyen, N. Hersch, A. Sechi, S. Joussen, B. Denecke, R. Merkel, B. Hoffmann, A. Dreser, U. Schnakenberg, A. Gillner and W. Wagner, *Biomaterials*, 2015, **61**, 316-326.
7. L. G. Xia, K. L. Lin, X. Q. Jiang, B. Fang, Y. J. Xu, J. Q. Liu, D. L. Zeng, M. L. Zhang, X. L. Zhang, J. Chang and Z. Y. Zhang, *Biomaterials*, 2014, **35**, 8514-8527.
8. X. N. Liu, R. L. Liu, B. Cao, K. Ye, S. Y. Li, Y. X. Gu, Z. Pan and J. D. Ding, *Biomaterials*, 2016, **111**, 27-39.
9. B. Y. Xu, G. B. Song, Y. Ju, X. Li, Y. H. Song and S. Watanabe, *J Cell Physiol*, 2012, **227**, 2722-2729.
10. F. Guilak, D. M. Cohen, B. T. Estes, J. M. Gimble, W. Liedtke and C. S. Chen, *Cell Stem Cell*, 2009, **5**, 17-26.
11. J. D. Humphrey, E. R. Dufresne and M. A. Schwartz, *Nat Rev Mol Cell Bio*, 2014, **15**, 802-812.
12. A. B. Faia-Torres, S. Guimond-Lischer, M. Rottmar, M. Charnley, T. Goren, K. Maniura-Weber, N. D. Spencer, R. L. Reis, M. Textor and N. M. Neves, *Biomaterials*, 2014, **35**, 9023-9032.
13. D. S. Harburger and D. A. Calderwood, *J Cell Sci*, 2009, **122**, 159-163.
14. A. Arjonen, J. Alanko, S. Veltel and J. Ivaska, *Traffic*, 2012, **13**, 610-625.
15. S. J. Shattil, C. Kim and M. H. Ginsberg, *Nat Rev Mol Cell Bio*, 2010, **11**, 288-300.
16. D. A. Calderwood, I. D. Campbell and D. R. Critchley, *Nat Rev Mol Cell Bio*, 2013, **14**, 503-517.
17. J. L. Guan, *Iubmb Life*, 2010, **62**, 268-276.
18. T. Roch, A. Kruger, K. Kratz, N. Ma, F. Jung and A. Lendlein, *Clin Hemorheol Micro*, 2012, **52**, 375-389.

19. W. W. Wang, N. Ma, K. Kratz, X. Xu, Z. D. Li, T. Roch, K. Bieback, F. Jung and A. Lendlein, *Clin Hemorheol Micro*, 2012, **52**, 357-373.
20. M. Bigerelle, S. Giljean and K. Anselme, *Acta Biomater*, 2011, **7**, 3302-3311.
21. M. A. Schwartz, *Cols Spring Harbor Perspect. Biol.*, 2010, **2**, a005066.
22. K. A. Kilian, B. Bugarija, B. T. Lahn and M. Mrksich, *P Natl Acad Sci USA*, 2010, **107**, 4872-4877.
23. I. Wierzbicka-Patynowski and J. E. Schwarzbauer, *J Cell Sci*, 2003, **116**, 3269-3276.
24. G. L. Lin, D. M. Cohen, R. A. Desai, M. T. Breckenridge, L. Gao, M. J. Humphries and C. S. Chen, *Febs Lett*, 2013, **587**, 763-769.
25. X. Zhao and J. L. Guan, *Adv Drug Deliver Rev*, 2011, **63**, 610-615.
26. C. T. Mierke, *Phys Biol*, 2013, **10**, 065005.
27. S. K. Mitra and D. D. Schlaepfer, *Curr Opin Cell Biol*, 2006, **18**, 516-523.
28. S. K. Mitra, D. Mikolon, J. E. Molina, D. A. Hsia, D. A. Hanson, A. Chi, S. T. Lim, J. A. Bernard-Trifilo, D. Ilic, D. G. Stupack, D. A. Cheresh and D. D. Schlaepfer, *Oncogene*, 2006, **25**, 5969-5984.
29. A. A. Abdeen, J. Lee, Y. Li and K. A. Kilian, *Regen. Eng. Transl. Med.*, 2017, **3**, 10.
30. R. Meili, A. T. Sasaki and R. A. Firtel, *Nat Cell Biol*, 2005, **7**, 334-335.
31. M. S. Song, L. Salmena and P. P. Pandolfi, *Nat Rev Mol Cell Bio*, 2012, **13**, 283-296.
32. S. Zimmermann and K. Moelling, *Science*, 1999, **286**, 1741-1744.
33. F. G. Teixeira, M. M. Carvalho, N. Sousa and A. J. Salgado, *Cell Mol Life Sci*, 2013, **70**, 3871-3882.
34. S. H. Ranganath, O. Levy, M. S. Inamdar and J. M. Karp, *Cell Stem Cell*, 2012, **10**, 244-258.
35. D. Drago, C. Cossetti, N. Iraci, E. Gaude, G. Musco, A. Bachi and S. Pluchino, *Biochimie*, 2013, **95**, 2271-2285.
36. C. Gallina, V. Turinetto and C. Giachino, *Stem Cells Int*, 2015, **2015**, 765846.
37. V. R. Burst, M. Gillis, F. Putsch, R. Herzog, J. H. Fischer, P. Heid, J. Muller-Ehmsen, K. Schenk, J. W. U. Fries, C. A. Baldamus and T. Benzing, *Nephron Exp Nephrol*, 2010, **114**, E107-E116.
38. M. Leiker, G. Suzuki, V. S. Iyer, J. M. Canty and T. Lee, *Cell Transplant*, 2008, **17**, 911-922.
39. E. J. Lee, H. W. Park, H. J. Jeon, H. S. Kim and M. S. Chang, *Regen Med*, 2013, **8**, 283-293.
40. R. A. Boomsma and D. L. Geenen, *Plos One*, 2012, **7**, e35685.
41. A. Hoeben, B. Landuyt, M. S. Highley, H. Wildiers, A. T. Van Oosterom and E. A. De Bruijn, *Pharmacol Rev*, 2004, **56**, 549-580.